COMMUNICATION

In vivo photoacoustic mapping of lymphatic systems with plasmon-resonant nanostars†‡

Chulhong Kim,§*ac* Hyon-Min Song,§*b* Xin Cai,*a* Junjie Yao,*a* Alexander Wei¶**b* and Lihong V. Wang¶**a*
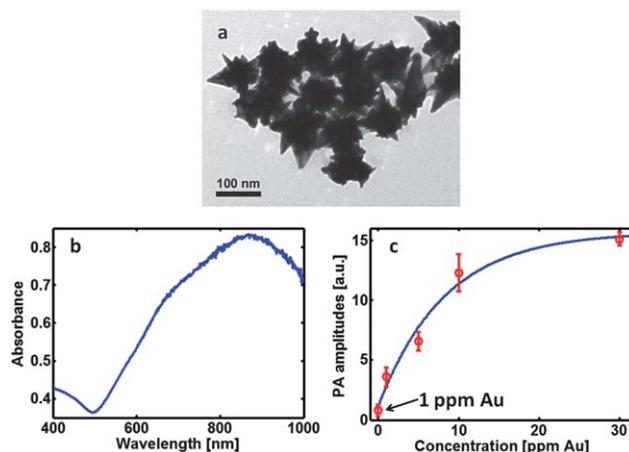
Plasmon-resonant nanostars (NSTs) provide excellent contrast enhancement for photoacoustic tomography. The high photoacoustic sensitivity of NSTs at near-infrared wavelengths enables their *in vivo* detection in rat sentinel lymph nodes and vessels, with direct application toward lymphangiography.

Noninvasive medical imaging systems have been widely used in clinics to improve diagnostic accuracy and treatment outcomes in cancer patients.[1] Along with the development of imaging techniques, molecular and nanosized contrast agents have been actively explored to improve detection sensitivity and specificity in biomedical imaging.[2] Here we demonstrate that plasmon-resonant nanostars (NSTs) are excellent contrast agents for *in vivo* photoacoustic tomography (PAT), with a detection limit at 1 ppm ($\sim$1 µg mL^{-1}) Au. Gold NSTs have a strong optical response at near-infrared (NIR) wavelengths, and have been recently deployed as contrast agents for optical imaging[3] and also as substrates for SERS and other plasmon-enhanced sensing modalities.[4] In this article, we use *in vivo* spectroscopic PAT to monitor the accumulation of NSTs in the sentinel lymph nodes (SLNs) of a rat specimen shortly after a footpad injection, which was later confirmed by *ex vivo* PAT and inductively coupled plasma mass spectrometry (ICP-MS).

PAT is a nonionizing, noninvasive, and high-resolution imaging technique that provides strong optical absorption contrast.[5] Since the spatial resolution of this technique typically depends on ultrasound (US) parameters, the imaging depth can be extended to the optical quasidiffusive or diffusive regime while keeping high resolution. The depth-to-resolution ratio of PAT (defined as the ratio of maximum penetration depth to depth resolution) is greater than 100 for all imaging depths. PAT can provide structural information (*e.g.*, vascular networks or melanomas) using the intrinsic PA contrast produced by hemoglobin or melanin, and also functional information based on total hemoglobin concentration, oxygen saturation, or blood flow.[5] Exogenous materials such as nanoparticles also play an important role by enhancing PA contrast for molecular imaging[6] and noninvasive SLN mapping.[7] The PA sensitivities for detecting organic dyes and nanoparticles range from 10 nM at 0.3 mm resolution ($\sim$1 fmol per imaging voxel) to 10 pM at 0.06 mm resolution ($\sim$0.1 attomole per imaging voxel).[5] Au-based nanoparticles have been approved by FDA as drug carriers or therapeutic agents for various phase-I clinical trials (*e.g.*, http://www.nanospectra.com). From a clinical perspective, conventional US array systems can be easily adapted to perform both PA and US imaging, and hand-held, array-based probes have recently been designed.[8]

Gold NSTs with an average span of 120 nm (Fig. 1a) were prepared by a seeded growth method as previously described, starting from either 13 nm core–shell Fe$_3$O$_4$@Au particles[3,9] (sample A) or from 8 nm Au particles[10] (sample B). Both samples were synthesized

aOptical Imaging Laboratory, Department of Biomedical Engineering, Washington University in St Louis, One Brookings Dr., St Louis, MO, USA. Fax: +1-314-935-7448; Tel: +1-314-935-6152

bDepartment of Chemistry, Purdue University, 560 Oval Dr., West Lafayette, IN, USA. Fax: +1-765-494-2039; Tel: +1-765-494-5257

cDepartment of Biomedical Engineering, University at Buffalo, The State University of New York, 328 Bonner Hall, Buffalo, NY, 14260, USA

Fig. 1 (a) TEM image of plasmon-resonant Au nanostars (NSTs, sample A). (b) Extinction spectrum of diluted sample A. The absorbance (arbitrary unit) of the Au nanostars is $\sim$0.75 at 767 nm. (c) A plot of photoacoustic (PA) amplitudes as a function of NST concentration (see ESI† for details).

using freshly prepared growth solution; NST growth was complete within 15 minutes after seed addition (see ESI† for details). The CTAB-stabilized NSTs were purified by treatment with a poly-styrenesulfonate solution to remove excess CTAB,[11] then resuspended in 1% bovine serum albumin (BSA) to produce NSTs in their final, biocompatible form. The extinction spectra of BSA-stabilized NSTs with and without magnetic cores (Fig. 1b and S1, ESI†) confirm their strong NIR activities, in accord with earlier reports.[3,11]

PAT imaging was performed in spectroscopic mode using a developed deep-reflection modality (see ESI† for details).[7] The PA sensitivity was calibrated using two Tygon® tubes, one filled with aqueous suspensions of NSTs at various concentrations, the other with defibrinated bovine blood. PA signals from plasmon-resonant NSTs in tissue phantoms (sample A) were detected at a concentration of 1 ppm Au with a signal-to-noise ratio of 4 (λ_{ex} = 767 nm; Fig. 1c). This detection limit corresponds roughly to NST concentrations in the femtomolar range, with 10^4 to 10^5 NSTs per imaging voxel (see ESI† for details).

The PA contrast was evaluated by performing a volumetric *in vivo* mapping of rat lymphatic systems (Fig. 2). Sprague-Dawley rats were anesthetized according to a standard protocol (see ESI† for details) with hair removed from the left axillary region in order to obtain control PA images, prior to the introduction of NSTs (Fig. 2a and d, top). The vascular networks passing through the axilla are clearly visible due to the intrinsic PA contrast of hemoglobin, however, neither the lymphatic vessels nor lymph nodes can be observed.

Rats were then inoculated with an injection of BSA-stabilized NSTs in the left footpad (0.1 mL of sample A, ~100 μg Au), and the left axilla was monitored by *in vivo* spectroscopic PAT. At 1.5 h post-injection, the SLN and lymphatic vessels (yellow) clearly stand out due to the exogenous contrast generated by the NSTs (Fig. 2b). The SLN is located 1.5 mm below the skin (Fig. S3, ESI†), but can be clearly resolved by subtracting the control PA image from the post-injection image (Fig. 2b). A volumetric rendering of the PA contrast reveals how the blood vessels and lymphatic vasculatures are interwoven (Fig. 2c and Movie S1, ESI†). The accumulation of NSTs in the SLN was visually confirmed after the *in vivo* imaging study, upon removal of the skin from the left axillary region (Fig. 2d, bottom). We note that Au NSTs without Fe_3O_4 cores produce comparable PA contrast (see below), as this is derived solely from their plasmon-resonant optical properties.
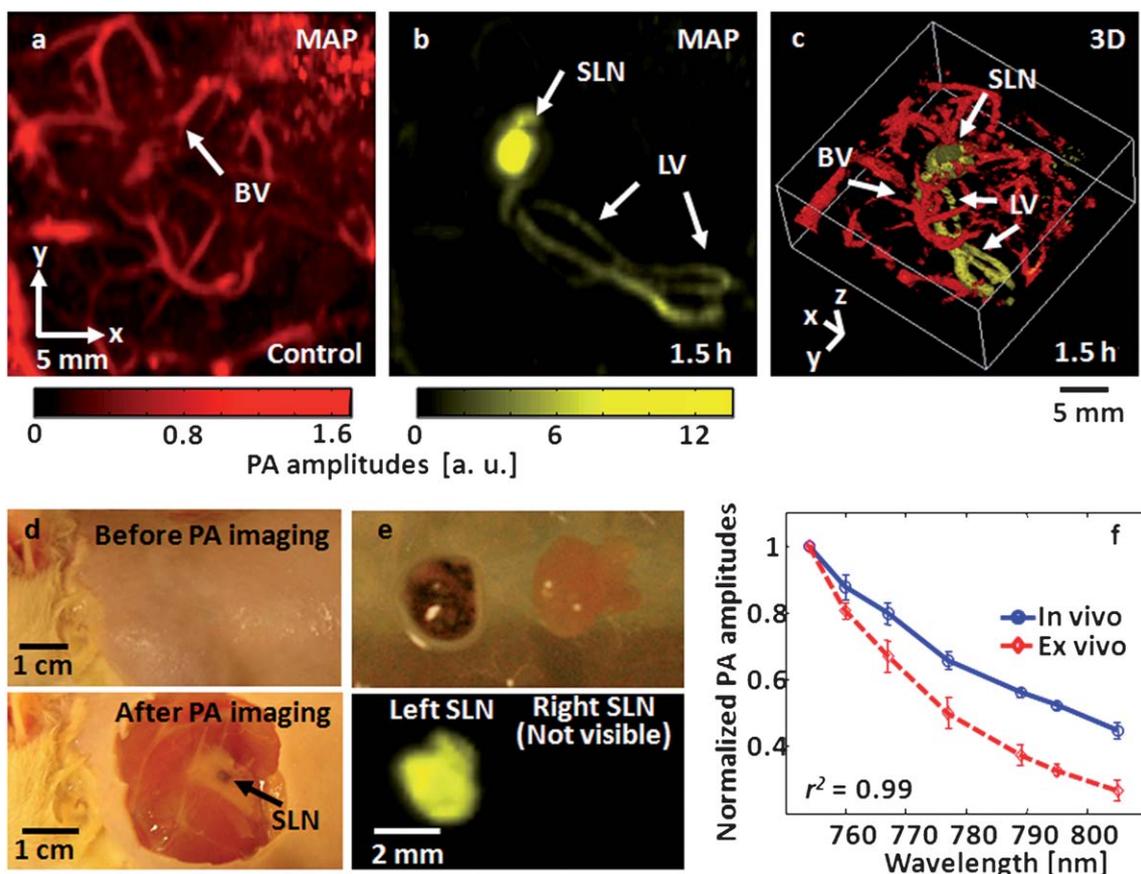
Fig. 2 *In vivo* photoacoustic (PA) mapping of rat lymphatic systems, enhanced using NSTs (sample A). (a) Control PA image acquired before NST injection, displaying only blood vessels (BV). (b) PA difference image acquired post-injection (*t* = 1.5 h), revealing the sentinel lymph node (SLN) and lymphatic vessels (LV). A separate intensity scale (yellow) was applied to the lymphatic system after subtraction of image (a). (c) 3D rendering of (b). (d) Photographs of the left axillary region before inoculation with NSTs (top) and after *in vivo* PA imaging (bottom), revealing the accumulation of NSTs in the SLN. (e) Photograph (top) and *ex vivo* PA image (bottom) of excised SLNs; the left axillary region (closest to the injection site) contains a visibly high concentration of NSTs, whereas the SLN from the right axillary region does not. (f) *In vivo* and *ex vivo* spectroscopic PA amplitudes measured within the SLNs, 1.5 h after inoculation with NSTs.
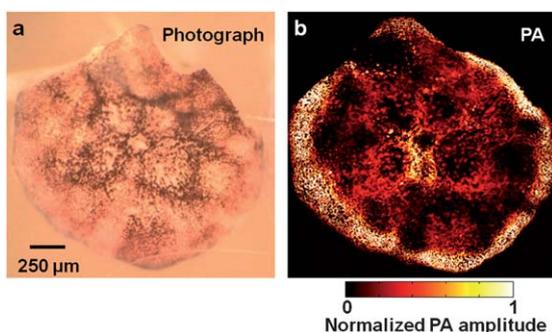
The SLNs from the left and right axillae were harvested for *ex vivo* spectroscopic PAT. Only the left SLN (closest to injection site) accumulated an appreciable amount of NSTs, as indicated by both visual inspection and PA imaging (Fig. 2e). The spectral amplitudes measured by *in vivo* and *ex vivo* imaging produced similar trends ($r^2 = 0.99$), confirming the SLN as the source of PA signal.

Ex vivo PA imaging was also performed at visible wavelengths ($\lambda_{ex} = 570$ nm) on lymph nodes containing gold NSTs (sample B) using optical-resolution PA microscopy (see Fig. 3 and ESI†).[12] In addition to confirming their strong PA contrast at shorter wavelengths, the microscopic PA image revealed the relative distribution and density of NSTs throughout the SLN. The NSTs appear to accumulate in both the subcapsular and trabecular sinuses, implying their diffusion into successive lymph nodes.

The PA image contrasts from *in vitro*, *in vivo*, and *ex vivo* studies are compared in Table 1, using an excitation wavelength of 767 nm. The image contrast is defined simply as $(S - B)/B$, where S is the mean PA signal from objects of interest (*e.g.*, SLNs or blood vessels) and B is the mean background signal. For *in vitro* imaging, the PA contrast of NSTs at 1000 ppm Au is ~10 times stronger than that of whole blood, whereas *in vivo* studies indicate the mean PA contrast of NSTs accumulated in SLNs (1.5 h after injection) to be ~3 times stronger than that of nearby blood vessels. The *ex vivo* PA contrast produced from NSTs in excised SLNs (an average weight of ~50 mg) was similar to that above; ICP-MS analysis indicated a loading of 42 ± 16 ppm Au, corresponding to a mean injected dose percentage (ID%) of ~2%. It should be noted that the NSTs will continue to migrate from the footpad into the lymphatic system and collect in the SLN over time, so the dosage of NSTs needed for lymph node detection is well below the amount used in this study.

Although *in vivo* and *ex vivo* spectroscopic PA imaging confirm the uptake of NSTs in the SLNs, it is worth mentioning that their excitation spectra do not coincide with the initial optical (extinction) spectrum of the NSTs in solution (Fig. 1b). Reasons for this discrepancy may be attributed as follows: (i) the NST extinction spectrum is defined in part by plasmon-resonant scattering, whereas PA imaging is mostly sensitive to optical absorption; (ii) the NSTs are likely to be aggregated upon accumulation in SLNs, causing significant changes in their collective optical response.[13] We note similar changes in the optical response of NSTs when dispersed into tissue phantoms (not shown).

Lymph node mapping has become an important objective in the detection and subsequent prevention of early stage metastases.[14] The

Table 1 Photoacoustic (PA) image contrast of NSTs derived from *in vitro*, *in vivo*, and *ex vivo* studies (sample A, $N = 3$)

	Blood	NSTs (ppm Au)
In vitro	5 ± 1	51 ± 3^a
In vivo	18 ± 4	59 ± 22^b
Ex vivo	—	44 ± 21^b

^{a} [NST] = 1000 ppm; mean and standard deviation. ^{b} NSTs in SLN; mean and standard error.

measurements above, in conjunction with the PA detection limit established in Fig. 1 (1 ppm Au), indicate that Au NSTs are well suited as contrast agents for lymphatic mapping by PAT. We note that the detection limit for NSTs is similar to that measured from other types of gold nanoparticles, but many orders of magnitude lower than those for single-walled carbon nanotubes coated with indocyanine green, when compared on a per particle basis.[15] The biocompatibility of colloidal Au is already well established, so the use of Au NSTs as PAT contrast agents may find promise in clinical cancer applications involving SLN detection.

In summary, we have demonstrated that plasmon-resonant NSTs can be used with volumetric spectroscopic PAT for non-invasive *in vivo* mapping of lymphatic systems. Subcutaneous injections of NSTs into rat footpads led to their drainage into SLNs and lymphatic vessels, enabling these to be visualized and distinguished from nearby blood vessels. Further improvements in exogenous PAT contrast are possible by introducing dynamic modes of contrast based on periodic signal modulation,[16] as recently demonstrated with magnetomotive NSTs[3,9] and also with Au-coated colloidal Fe_3O_4.[17] Steps taken in this direction may accelerate the development of NSTs and other nanoparticles as PAT-based contrast agents for lymphangiography.

Notes and references

1 W. Cai and X. Chen, *J. Nucl. Med.*, 2008, **49**, 113S.
2 C. Kim, K. H. Song, F. Gao and L. V. Wang, *Radiology*, 2010, **255**, 442; C. Kim, R. Qin, J. S. Xu, L. V. Wang and R. Xu, *J. Biomed. Opt.*, 2010, **15**, 010510; T. N. Erpelding, C. Kim, M. Pramanik, L. Jankovic, K. Maslov, Z. Guo, J. A. Margenthaler, M. D. Pashley and L. V. Wang, *Radiology*, 2010, **256**, 102.
3 H.-M. Song, Q. Wei, Q. K. Ong and A. Wei, *ACS Nano*, 2010, **4**, 5163; J. S. Aaron, E. de la Rosa, K. Travis, N. Harrison, J. Burt, M. José-Yacamán and K. Sokolov, *Opt. Express*, 2008, **16**, 2153; Z. Wang, J. Zhang, J. M. Ekman, P. J. A. Kenis and Y. Lu, *Nano Lett.*, 2010, **10**, 1886.
4 C. G. Khoury and T. Vo-Dinh, *J. Phys. Chem. C*, 2008, **112**, 18849; E. S. Allgeyer, A. Pongan, M. Browne and M. D. Mason, *Nano Lett.*, 2009, **9**, 3816; L. Rodríguez-Lorenzo, R. A. Álvarez-Puebla, I. Pastoriza-Santos, S. Mazzucco, O. Stephan, M. Kociak, L. M. Liz-Márzan and F. J. G. de Abajo, *J. Am. Chem. Soc.*, 2009, **131**, 4616.
5 L. V. Wang, *Nat. Photonics*, 2009, **3**, 503; C. Kim, C. Favazza and L. V. Wang, *Chem. Rev.*, 2010, **110**, 2756.
6 C. Kim, E. C. Cho, J. Chen, K. W. Hyun, L. Au, C. Favazza, Q. Zhang, C. M. Cobley, F. Gao, Y. Xia and L. V. Wang, *ACS Nano*, 2010, **4**, 4559; P. Li, C. C. Wang, D. Shieh, C. Wei, C. Liao, C. Poe, S. Jhan, A. Ding and Y. Wu, *Opt. Express*, 2008, **16**, 18605.
7 K. H. Song, C. Kim, C. M. Cobley, Y. Xia and L. V. Wang, *Nano Lett.*, 2009, **9**, 183; K. H. Song, C. Kim, K. Maslov and L. V. Wang, *Eur. J. Radiol.*, 2009, **70**, 227.
8 C. Kim, T. N. Erpelding, K. Maslov, L. Jankovic, W. J. Walter, L. Song, S. Achilefu, J. A. Margenthaler, M. D. Pashley and L. V. Wang, *J. Biomed. Opt.*, 2010, **15**, 046010; C. Kim, T. N. Erpelding, L. Jankovic, M. D. Pashley and L. V. Wang, *Opt. Express*, 2010, **1**, 278.

Fig. 3 (a) Brightfield optical microscopy of an excised SLN, harvested from a rat specimen 1.5 h after inoculation with solid Au NSTs (sample B). (b) *Ex vivo* PA image of the excised SLN, using a micro-PAT system operating at shorter wavelengths ($\lambda_{ex} = 570$ nm).

9 Q. Wei, H.-M. Song, A. P. Leonov, J. B. Hale, D. Oh, Q. K. Ong, K. P. Ritchie and A. Wei, *J. Am. Chem. Soc.*, 2009, **131**, 9728.
10 C. L. Nehl, H. Liao and J. H. Hafner, *Nano Lett.*, 2006, **6**, 683.
11 A. P. Leonov, J. Zheng, J. D. Clogston, S. T. Stern, A. K. Patri and A. Wei, *ACS Nano*, 2008, **2**, 2481.
12 S. Hu and L. V. Wang, *J. Biomed. Opt.*, 2010, **15**, 011101.
13 Q. Wei and A. Wei, in *Supramolecular Chemistry of Organic–Inorganic Hybrid Materials*, ed. K. Rurack and R. M. Mañez, Wiley and Sons, New York, 2010, p. 319.
14 A. J. Cochran, A. A. Roberts and T. Saida, *Int. J. Clin. Oncol.*, 2003, **8**, 139; M. Gipponi, N. Solari, F. C. Di Somma, S. Bertoglio and F. Cafiero, *J. Surg. Oncol.*, 2004, **85**, 171.
15 A. Zerda, Z. Liu, S. Bodapati, R. Teed, S. Vaithilingam, B. T. Khuri-Yakub, X. Chen, H. Dai and S. S. Gambhir, *Nano Lett.*, 2010, **10**, 2168.
16 Q. Wei and A. Wei, *Chem.–Eur. J.*, 2011, **17**, 1080.
17 Y. Jin, C. Jia, S.-W. Huang, M. O'Donnell and X. Gao, *Nat. Commun.*, 2010, **1**, 1.